# Nonequilibrium $GW$ + EDMFT: Antiscreening and Inverted Populations from Nonlocal Correlations

Denis Golež,[1] Lewin Boehnke,[1] Hugo U. R. Strand,[1] Martin Eckstein,[2] and Philipp Werner[1]
[1]Department of Physics, University of Fribourg, 1700 Fribourg, Switzerland
[2]Max-Planck Institute for the Structure and Dynamics of Matter, 22761 Hamburg, Germany
(Received 16 February 2017; published 15 June 2017)

We study the dynamics of screening in photodoped Mott insulators with long-ranged interactions using a nonequilibrium implementation of the $GW$ plus extended dynamical mean-field theory formalism. Our study demonstrates that the complex interplay of the injected carriers with bosonic degrees of freedom (charge fluctuations) can result in long-lived transient states with properties that are distinctly different from those of thermal equilibrium states. Systems with strong nonlocal interactions are found to exhibit a self-sustained population inversion of the doublons and holes. This population inversion leads to low-energy antiscreening which can be detected in time-resolved electron-energy-loss spectra.

DOI: 10.1103/PhysRevLett.118.246402

The development of time-resolved spectroscopic techniques provided important insights into the properties of complex materials [1–5], where charge, spin, orbital, and lattice degrees of freedom are intertwined. A particularly exciting prospect is the nonequilibrium manipulation of material properties on electronic time scales and the exploration of transient states that cannot be realized under equilibrium conditions. Prominent examples of this development are the laser-induced switching to a hidden state [6] in $1T$-$TaS_2$ and an apparent increase of the superconducting $T_c$ in phonon-driven cuprates and fulleride superconductors [7,8].

Essential for the understanding of such experiments and phenomena is the ability to simulate relevant model systems using techniques that capture correlation effects in highly nonthermal states. Of particular importance is a proper description of the time-dependent screening processes, which determine the interaction parameters in such model Hamiltonians. The photoinduced change of screening was considered, e.g., as the cause of the collapse of the band gap in $VO_2$ [9] and the enhancement of excitonic order in $Ta_2NiSe_5$ [10]. Moreover, screening originates from charge fluctuations, which, similar to other bosonic modes like phonons [11–14] or spin fluctuations [15,16], profoundly affect the relaxation pathway of the electronic distribution. As we will show in this Letter, the fermionic dynamics and the bosonic screening modes are so strongly coupled, that their mutual interplay can lead to long-lived transient states which are entirely different from those characterizing equilibrium phases. These nonthermal states, with partially inverted populations, thus provide an intriguing pathway to novel light-induced properties.

A promising formalism to address these questions in strongly correlated solids is the combination of the $GW$ method and the extended dynamical mean-field theory ($GW$ + EDMFT) [17]. Hedin's $GW$ method [18,19] is a weak-coupling approach in which the self-energy is approximated by the product of the Green's function $G$ and the screened interaction $W$. It captures nonlocal physics resulting from charge fluctuations, like screening, plasmonic collective modes, and charge density waves. It however fails to describe strong correlation effects, like the Mott metal-insulator transition, which in turn are well described by the nonperturbative dynamical mean-field theory (DMFT) [20] and extended DMFT (EDMFT) [21]. $GW$ + EDMFT is a fully diagrammatic approach, which allows a self-consistent calculation of the screened interaction and its effect on the electronic properties in systems with long-ranged Coulomb interactions. In combination with a $GW$-based *ab initio* calculation it enables a parameter-free simulation of weakly and strongly correlated materials. The recent equilibrium application of $GW$ + EDMFT to model systems [22–24] and real materials [25] demonstrated the importance of dynamical screening effects originating from nonlocal interactions, e.g., for the proper interpretation of spectral features such as Hubbard bands and plasmon satellites. Here, we develop the nonequilibrium extension of the $GW$ + EDMFT formalism and use it to study the effect of nonlocal interactions on the transient states and the relaxation dynamics of photoexcited carriers in Mott insulators.

As a simple but generic system with intersite interactions, we consider the single-band $U$-$V$ Hubbard model on the two-dimensional square lattice:

$$H(t) = -J\sum_{\langle ij\rangle\sigma}(e^{i\phi_{ij}(t)}c^{\dagger}_{i\sigma}c_{j\sigma} + \text{H.c.}) - \mu\sum_i n_i + \sum_i U\left(n_{i\uparrow}-\frac{1}{2}\right)\left(n_{i\downarrow}-\frac{1}{2}\right) + \sum_{\langle ij\rangle} V(n_i-1)(n_j-1), \tag{1}$$

 

where $c_{i\sigma}$ is the annihilation operator of a fermion with spin $\sigma$ on lattice site $i$, $n_i = n_{i\uparrow} + n_{i\downarrow}$, $\mu$ is the chemical potential, $U$ is the on-site interaction, and $V$ is the interaction between electrons on neighboring sites [26]. The hopping integral $Je^{i\phi_{ij}(t)}$ (restricted to nearest neighbors) has a time-dependent Peierls phase $\phi_{ij}(t) = \int_0^t d\bar{t}\,\vec{E}(\bar{t})(\vec{r}_i - \vec{r}_i)$ originating from an in-plane electric field $\vec{E}(t)$. In the following, we will use the hopping amplitude $J \equiv 1$ as the unit of energy and rewrite the interaction as $\frac{1}{2}\sum_{ij} v_{ij}\tilde{n}_i\tilde{n}_j$, where $\tilde{n} = n - 1$ is the density fluctuation operator and $v_{ij} = U\delta_{ij} + V\delta_{\langle ij\rangle}$.

The dynamics of the system is described in terms of the momentum-dependent electron Green's function $G_k(t,t') = -i\langle T_C c_k(t) c_k^\dagger(t')\rangle$ and the charge correlation function $\chi_q(t,t') = -i\langle T_C \tilde{n}_q(t)\tilde{n}_{-q}(t')\rangle$, which determines the (inverse) dielectric function $\varepsilon_q^{-1} = 1 + v_q * \chi_q$ and the screened interaction $W_q = \varepsilon_q^{-1} * v_q$, where $v_q$ is the Fourier transform of $v_{ij}$. In nonequilibrium, all quantities depend on two time arguments, or equivalently on time and frequency, and the $*$ product denotes a convolution in time [27].

To solve the extended Hubbard model in Eq. (1), we resort to the $GW$ + EDMFT approximation [17], which can be derived using the Almbladh functional [34]. Nonlocal self-energy contributions for electrons and bosonic charge fluctuations are treated within the lowest-order expansion of the functional (the $GW$ formalism), while the local contributions are included to all orders, by solving an auxiliary Anderson-Holstein impurity model with a self-consistently determined bosonic and fermionic bath. As a Green's-function-based formalism, $GW$ + EDMFT is not restricted to equilibrium or quasistatic problems but can handle highly excited states. The derivation of the nonequilibrium formalism within the Keldysh framework is analogous to the equilibrium version [22,35] and is presented in the Supplemental Material [28].

While powerful and numerically exact methods [36] exist for the solution of the $GW$ + EDMFT equations in equilibrium, the application to nonequilibrium problems requires additional approximations at the level of the impurity solver. Since our goal is to study photodoped Mott insulators, we use a perturbative solver that combines a self-consistent hybridization expansion [at first (second) order known as the noncrossing (one-crossing) approximation NCA (OCA) [37–39]] with a weak-coupling expansion in the retarded density-density interactions. For technical aspects of the implementation, see Ref. [40]. As a benchmark, we show in Fig. 1(a) a comparison of the Matsubara component of the Green's functions $G^{\mathrm{Mat}}(\tau)$ for $U = 10.5$, $V = 1.5$, and inverse temperature $\beta = 20$. [In the following, local (nonlocal) correlators are distinguished by the absence (presence) of a subscript momentum label.] The NCA is found to overestimate the insulating nature of the solution [41,42], as seen from $G^{\mathrm{Mat}}(\beta/2)$, which can be taken as a measure for the spectral weight at the Fermi level. While this is a known artifact of the NCA [41,42], the OCA substantially improves the accuracy of the solution compared to numerically exact Monte Carlo results [36]. Furthermore, the finite-temperature metal-insulator transition is a crossover in the NCA description and becomes first order in the OCA solution; see Fig. 1(d). In the Mott phase, which we study here, the NCA and OCA, however, yield qualitatively similar results, and we will resort to the numerically more tractable NCA in the following.

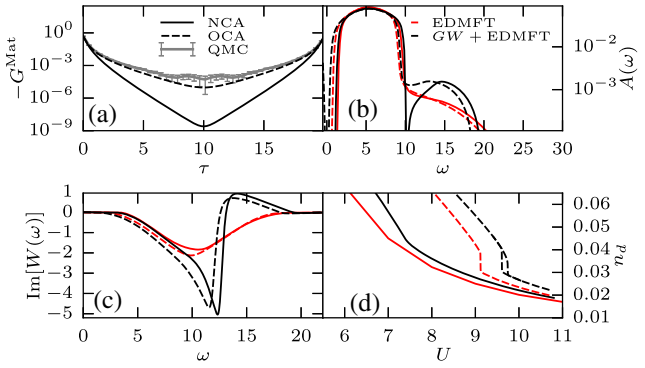


FIG. 1. Equilibrium results for $U = 10.5$, $V = 1.5$, and $\beta = 20$. (a) Comparison of the Matsubara time component of the Green's function $G^{\mathrm{Mat}}(\tau)$ obtained from NCA, OCA, and numerically exact Monte Carlo simulations for $U = 10.5$. (b) Spectral functions obtained from different approximations. Solid (dashed) lines correspond to the NCA (OCA) solution. (c) Imaginary part of the screened interaction $W(\omega)$ obtained from different approximations. (d) Double occupation $n_d$ near the metal-insulator transition or crossover. A coexistence region exists in the OCA.

In the spectral function, shown in Fig. 1(b), the additional nonlocal $GW$ self-energy contributions in $GW$ + EDMFT strongly enhance the plasmonic sideband at $\omega \approx \frac{3}{2}U$ and result in a slight reduction of the gap size compared to the EDMFT. The inclusion of the nonlocal $GW$ diagrams in the $GW$ + EDMFT approximation leads to a more metallic solution, since nonlocal correlations (in particular, the nonlocal Fock term [24]) enhance the effective bandwidth. Also, the local (momentum-averaged) screened interaction $W$ is modified by the inclusion of the nonlocal polarization [Fig. 1(c)]. A noticeable feature is the strong enhancement of the plasmonic peak at $\omega \approx 12$ in comparison to the EDMFT. A drawback of our approximate solver is evident at energies above the plasmon peak, where $\mathrm{Im}[W]$ exhibits positive spectral weight, which is unphysical in thermal equilibrium. This problem arises because the NCA and OCA self-energies and polarizations are approximate strong-coupling solutions, which miss some of the local $GW$ diagrams. Numerically, we found that these artifacts are most pronounced deep in the Mott phase, while close to the MIT transition and in the correlated metal $\mathrm{Im}[W(\omega)]$

exhibits the expected analytical properties. Since the unphysical spectral weight appears only at very high energies, we believe that it is not crucial for the following discussion, which focuses on the low-energy screening properties of photodoped systems.

We now turn to the effect of nonlocal fluctuations on the relaxation dynamics after an electric field excitation. By applying a short pulse $E(t) = E_0 e^{-4.6(t-t_0)^2/t_0^2} \sin[\omega(t-t_0)]$ with frequency $\omega = U$ and appropriately tuned amplitude $E_0$, a certain density of holon-doublon pairs is created. The width of the pulse $t_0 = 2\pi n/\omega$ is chosen such that the envelope accommodates $n = 2$ electric field cycles. Deep in the Mott phase, the recombination of the holons and doublons after photoexcitation is strongly suppressed [37,43,44]. The photoexcited doublons can, however, relax within the upper Hubbard band, which manifests itself in the evolution of the kinetic energy. If the gap is small compared to the width of the Hubbard bands, the thermalization process, which involves impact ionization [45], leads to an *increase* in the number of doublons $n_d$; see the EDMFT results (dashed lines) in Fig. 2(a). As already discussed in Ref. [40], the inclusion of the nonlocal interactions on the EDMFT level decreases the relaxation times, due to the coupling to bosonic excitations (collective charge fluctuations). This picture remains valid if we include nonlocal self-energy and polarization effects in $GW$ + EDMFT but only if the nearest-neighbor interaction $V$ is small ($V \lesssim 0.5$). For larger values of $V$ (but still smaller than the critical value for the charge order transition), the double occupancy starts to *decrease*, which indicates that doublon-holon recombination occurs in the system; see the solid lines in Fig. 2(a). Furthermore, the kinetic energy *increases* during the relaxation process, illustrated in Fig. 2(b), which is also intriguingly different from the behavior reported in previous photodoping studies [12,40,45].

In order to gain further insight into this intermediate $V$ regime, we calculate the time and frequency-resolved spectral function of the system. After the pulse excitation of the system, the spectral function $A(t,\omega) = -(1/\pi)\mathrm{Im}[G^R(t,\omega)]$ remains almost unchanged, while the occupied density of states $N(t,\omega) = \mathrm{Im}[G^<(t,\omega)]/2\pi i$ shows an increase of roughly 1% in the occupancy of the upper Hubbard band [46]; see Fig. 3(a). In agreement with the evolution of the kinetic energy, we observe a shift of the excited doublons toward *higher energies*, in contrast to previous DMFT and EDMFT studies [12,40,45] that consistently showed a relaxation of doublons to the lower edge of the upper Hubbard band. This $GW$ + EDMFT evolution eventually results in a population inversion, as illustrated by the distribution function $f(t,\omega) = -2\mathrm{Im}[G^<(t,\omega)]/\mathrm{Im}[G^R(t,\omega)]$ shown in Fig. 3(b). We note again that this behavior is observed only for a sufficiently large nonlocal interaction $V$.

The efficient recombination of doublon-hole pairs and the population inversion within $GW$ + EDMFT can be understood by considering the two-particle properties, namely, the screened interaction $W$ and the charge susceptibility $\chi_q$. The time evolution of the local component of the screened interaction $W^{R,<}(t,\omega)$ for $U = 10.5$, $V = 1.5$ is shown in Fig. 3(d). In agreement with the previous EDMFT results, low-energy screening channels appear as a consequence of photodoping [40]. The main difference in $GW$ + EDMFT is that the imaginary part of $W^R(t,\omega)$ changes sign as the system evolves into the population-inverted state. Since EDMFT and $GW$ + EDMFT differ in the inclusion of nonlocal fluctuations, we can qualitatively understand these results by evaluating the nonlocal charge susceptibility through the particle-hole bubble contribution to the polarization. In the stationary case, the latter can be written as $\chi_q^R = \Pi_q^R[1 - v_q\Pi_q^R]^{-1}$, where the polarization $\Pi_q^R$ is given by

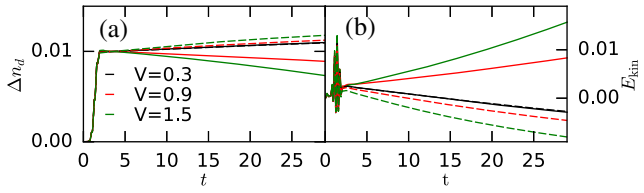


FIG. 2. Time evolution of the double occupancy $n_d$ (a) and kinetic energy (b) after the photoexcitation in EDMFT (dashed lines) and $GW$ + EDMFT (solid lines) for different nonlocal interactions $V$ at fixed density $\Delta n_d = 0.01$ of photoexcited carriers after the pulse. The local interaction is $U = 10.5$.

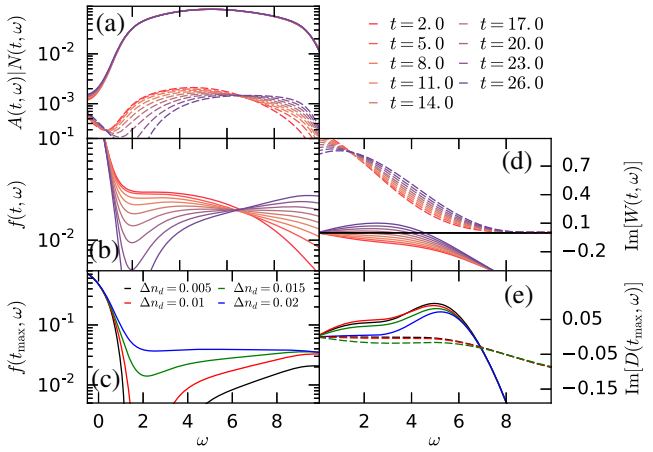


FIG. 3. (a) Time evolution of the spectral function (solid lines) and occupation (dashed lines) after the electric field excitation. (b) The distribution function illustrates the evolution into the self-sustained inverted population state. (c) Distribution functions for $t_{\mathrm{max}} = 24$ and different excitation strengths. (d) Time evolution of the screened interaction $W^R(t,\omega)$ (solid lines) and its lesser component (boson occupancy, dashed lines) $W^<(t,\omega)$ in the inverted population regime. (e) Imaginary part of the impurity effective interaction $\mathrm{Im}[D^R(t_{\mathrm{max}},\omega)]$ in EDMFT (dashed lines) and $GW$ + EDMFT (solid lines) for different excitations strengths. The pulse frequency is $\omega = U = 10.5$, the pulse amplitude is $E_0 = 2$ [except in (c)], and $V = 1.5$.

$$\Pi_q^R(\omega) = \sum_{k,\omega_1,\omega_2} A_k(\omega_1) A_{k-q}(\omega_2) \frac{f(\omega_1) - f(\omega_2)}{\omega - (\omega_1 - \omega_2)}, \quad (2)$$

which, in the case of well-defined quasiparticles and thermal distributions $f$, reduces to the Lindhard formula. By exciting doublon-hole pairs in a Mott insulator, we temporarily create an inverted population in some energy range. By changing the Fermi-Dirac distribution function $f(\omega)$ in Eq. (2) to a partially inverted distribution function $\tilde{f}(\omega)$, we can change the sign of the numerator in $\chi_q^R$ within a certain energy range. To illustrate this idea, we evaluate $\chi_q^R(\omega)$ using the Hubbard I approximation, where the lattice self-energy is approximated by the atomic limit self-energy. The resulting inverse dielectric function is shown in Fig. 4(a), where $\mathrm{Im}[\varepsilon_q^{-1}(t,\omega)] = v_q \mathrm{Im}[\chi_q^R(t,\omega)]$. This leads to maximum spectral weight at the $\Gamma$ point and $\omega \approx U$, which corresponds to charge excitations across the Mott gap. The lowest (highest) energies $U \pm W$ for which the imaginary part of the susceptibility $\mathrm{Im}[\chi_q^R(\omega)]$ has nonzero weight are at the $X$ point [$q = (\pi, \pi)$] [47]. In the case of the inverted population [see Fig. 4(c)], the numerator in Eq. (2) becomes negative at frequencies corresponding to the energy width of the inverted regions, which leads to a negative spectral weight $-v_q \mathrm{Im}[\chi_q^R(\omega)] < 0$. These considerations show that the inclusion of nonlocal dynamical screening via the polarization bubble in $GW$ + EDMFT is crucial for the appearance of the antiscreening phenomenon.

In contrast to the fermionic case, negative spectral weight in a steady state bosonic spectral function is not unphysical. The simplest example is a free oscillator, whose frequency suddenly turns unstable ($\omega_0 < 0$). Although there is no stable thermal equilibrium for $\omega_0 < 0$, the transient state remains well defined, and its negative spectral weight reflects the possibility to increase fluctuations by emitting energy to the environment. The change of the sign of $\mathrm{Im}[\chi_q(\omega)]$ in the photodoped Mott insulator thus indicates a negative attenuation of charge fluctuations, which enable the system to emit low-energy bosons to gain energy in the single-particle sector. This also explains the unusual increase of the kinetic energy of the photodoped carriers and the population inversion. A similar change in the sign of the susceptibilities was previously observed in models which are driven by (time-periodic) external fields [48,49]. The intriguing observation in the present case is that the inverted population of the electronic states and the negative charge susceptibility mutually support each other (because the softening of charge fluctuations is caused by the change of the fermionic distribution), so that the peculiar state is self-sustained and stable as long as doublon-hole recombination processes inject energy into the bosonic subsystem.

A related population inversion was recently discussed in a study of Hirsch's dynamic Hubbard model [50,51], although at unusually strong electron-phonon couplings. In the present case, the relevant strength $\lambda$ of the electron-boson coupling can be estimated from the density of states $D(t,\omega)$ of the bosonic modes in the auxiliary Anderson-Holstein impurity model (i.e., the boson-mediated density-density interaction) as $\lambda = \int d\omega \sqrt{|\mathrm{Im}D(\omega)|\omega}$ [22,40]. As shown in Fig. 3(e), in $GW$ + EDMFT, $\mathrm{Im}|D(t,\omega)|$ features a pronounced peak at the energy of the gap size $\omega \approx 6$, which corresponds to a very strong electron-boson coupling ($\lambda \approx 1.9$ for the largest value of $E$ plotted in the figure, if the integration range is chosen as $0 \le \omega \le 8$).

Experimental probes which could be used to detect the peculiar charge fluctuation region are electron-energy-loss spectroscopy (EELS) [52,53] and optical conductivity measurements [1]. The optical conductivity measures the frequency-dependent optical constant near the $\Gamma$ point [29,54], while the EELS signal $-\mathrm{Im}[v_q \varepsilon_q^{-1}(t,\omega)] = -v_q^2 \mathrm{Im}[\chi_q^R(t,\omega)]$ measures the difference between the dielectric loss and gain (in equilibrium and at low temperatures, there is only loss). The generalization of EELS to the nonequilibrium situation, along the lines of the derivation of the time-dependent photoemission formula [29–31], is presented in the Supplemental Material [28]. The closely related inverse dielectric constant $\varepsilon_q^{-1}(t,\omega)$ shows a similar structure in $GW$ + EDMFT as in the Hubbard I approximation; see Figs. 4(a) and 4(d). In particular, there is a pronounced maximum at the $\Gamma$ point at $\omega \approx U$ and dispersive bands with a minimal energy around the $X$ point. Immediately after the excitation, the weight in the subgap region is increased in agreement with

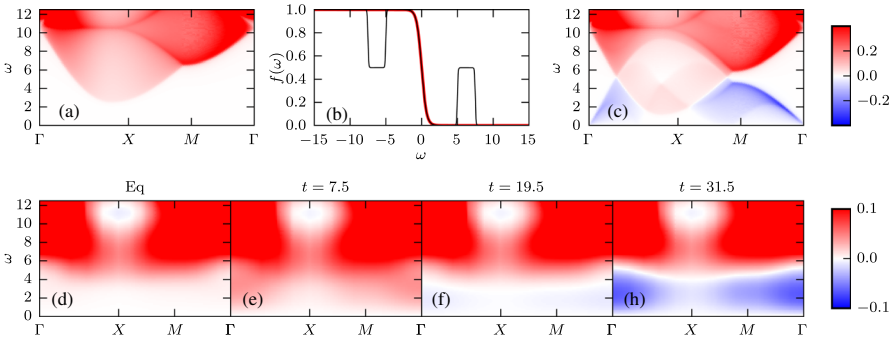


FIG. 4. Top panels: Imaginary part of the inverse dielectric function $-\mathrm{Im}[\varepsilon_q^{-1}(\omega)]$ obtained in the Hubbard I approximation for the thermal (a) and nonthermal (c) distribution functions shown in (b). Bottom panels: $GW$ + EDMFT results for $-\mathrm{Im}[\varepsilon_q^{-1}(t,\omega)]$ in equilibrium (d) and in the photoexcited system at indicated time delays (e)–(h). The pulse frequency is $\omega = U = 10.5$, the pulse amplitude is $E_0 = 2$, and $V = 1.5$.

previous EDMFT results [40]; see Fig. 4(e). The initial increase in the screening in the subgap region, however, gives way to a negative spectrum as the inverted doublon population is formed [Figs. 4(f)–4(h)] and the bosonic degrees of freedom also evolve into an inverted state. In this situation, the energy gain for the probe electron at a certain energy in the EELS experiment is larger than the loss.

In conclusion, the nonequilibrium $GW+\mathrm{EDMFT}$ simulation revealed a self-sustained and long-lived transient population inversion as a result of the nontrivial energy exchange between doublons, holons, and charge fluctuations. The existence of such a state provides an intriguing path to stabilize different types of light-induced order, which will be the subject of future investigations. Apart from these insights into the nonequilibrium properties of systems with nonlocal Coulomb interactions, our work represents an important step in the development of *ab initio* simulation approaches for correlated systems in nonequilibrium states. The $GW+\mathrm{EDMFT}$ method implemented here features a fully consistent treatment of correlation and screening effects and can, in principle, be combined with material-specific input from *ab initio GW* calculations within a multitier approach analogous to the scheme recently demonstrated for equilibrium systems in Ref. [25].

The calculations have been performed on the Beo04 cluster at the University of Fribourg. D. G., L. B., H. U. R. S., and P. W. have been supported by European Research Council (ERC) Starting Grant No. 278023 and ERC Consolidator Grant No. 724103, and the Swiss National Science Foundation through NCCR MARVEL and Grant No. 200021-165539. M. E. acknowledges support by the Deutsche Forschungsgemeinschaft within the Sonderforschungsbereich 925 (Project No. B4).

[1] C. Giannetti, M. Capone, D. Fausti, M. Fabrizio, F. Parmigiani, and D. Mihailovic, Adv. Phys. **65**, 58 (2016).
[2] S. D. Conte, C. Giannetti, G. Coslovich, F. Cilento, D. Bossini, T. Abebaw, F. Banfi, G. Ferrini, H. Eisaki, M. Greven, A. Damascelli, D. van der Marel, and F. Parmigiani, Science **335**, 1600 (2012).
[3] S. D, Conte *et al.*, Nat. Phys. **11**, 421 (2015).
[4] A. F. Kemper, M. A. Sentef, B. Moritz, T. P. Devereaux, and J. K. Freericks, arXiv:1609.00087.
[5] O. P. Matveev, A. M. Shvaika, T. P. Devereaux, and J. K. Freericks, Phys. Rev. B **94**, 115167 (2016).
[6] L. Stojchevska, I. Vaskivskyi, T. Mertelj, P. Kusar, D. Svetin, S. Brazovskii, and D. Mihailovic, Science **344**, 177 (2014).
[7] S. Kaiser *et al.*, Phys. Rev. B **89**, 184516 (2014).
[8] M. Mitrano *et al.*, Nature (London) **530**, 461 (2016).
[9] D. Wegkamp *et al.*, Phys. Rev. Lett. **113**, 216401 (2014).
[10] S. Mor, M. Herzog, D. Golež, P. Werner, M. Eckstein, N. Katayama, M. Nohara, H. Takagi, T. Mizokawa, C. Monney, and J. Stähler, arXiv:1608.05586.
[11] P. B. Allen, Phys. Rev. Lett. **59**, 1460 (1987).
[12] P. Werner and M. Eckstein, Phys. Rev. B **88**, 165108 (2013).
[13] D. Golež, J. Bonča, L. Vidmar, and S. A. Trugman, Phys. Rev. Lett. **109**, 236402 (2012).
[14] F. Dorfner, L. Vidmar, C. Brockt, E. Jeckelmann, and F. Heidrich-Meisner, Phys. Rev. B **91**, 104302 (2015).
[15] D. Golež, J. Bonča, M. Mierzejewski, and L. Vidmar, Phys. Rev. B **89**, 165118 (2014).
[16] M. Eckstein and P. Werner, Sci. Rep. **6**, 21235 (2016).
[17] S. Biermann, F. Aryasetiawan, and A. Georges, Phys. Rev. Lett. **90**, 086402 (2003).
[18] L. Hedin, Phys. Rev. **139**, A796 (1965).
[19] F. Aryasetiawan and O. Gunnarsson, Rep. Prog. Phys. **61**, 237 (1998).
[20] A. Georges, G. Kotliar, W. Krauth, and M. J. Rozenberg, Rev. Mod. Phys. **68**, 13 (1996).
[21] P. Sun and G. Kotliar, Phys. Rev. B **66**, 085120 (2002).
[22] T. Ayral, S. Biermann, and P. Werner, Phys. Rev. B **87**, 125149 (2013).
[23] L. Huang, T. Ayral, S. Biermann, and P. Werner, Phys. Rev. B **90**, 195114 (2014).
[24] T. Ayral, S. Biermann, P. Werner, and L. Boehnke, arXiv:1701.07718.
[25] L. Boehnke, F. Nilsson, F. Aryasetiawan, and P. Werner, Phys. Rev. B **94**, 201106 (2016).
[26] The extension to longer-ranged interactions is straightforward [23] and does not lead to qualitatively new physics.
[27] For a precise definition of time-ordered correlation functions on the Keldysh contour, see Supplemental Material [28].
[28] See Supplemental Material at http://link.aps.org/supplemental/10.1103/PhysRevLett.118.246402 for the functional derivation of the nonequilibrium $GW+$ EDMFT scheme and the interpretation of EELS spectra, which includes Refs. [29–33].
[29] M. Eckstein and M. Kollar, Phys. Rev. B **78**, 205119 (2008).
[30] J. K. Freericks, H. R. Krishnamurthy, and T. Pruschke, Phys. Rev. Lett. **102**, 136401 (2009).
[31] F. Randi, D. Fausti, and M. Eckstein, Phys. Rev. B **95**, 115132 (2017).
[32] L. P. Kadanoff and G. Baym, *Quantum Statistical Mechanics: Green's Function Methods in Equilibrium and Nonequilibrium Problems* (Benjamin, New York, 1962).
[33] R. Chitra and G. Kotliar, Phys. Rev. B **63**, 115110 (2001).
[34] C. O. Almbladh, U. v. Barth, and R. V. Leeuwen, Int. J. Mod. Phys. B **13**, 535 (1999).
[35] D. Hügel, P. Werner, L. Pollet, and H. U. R. Strand, Phys. Rev. B **94**, 195119 (2016).
[36] P. Werner and A. J. Millis, Phys. Rev. Lett. **104**, 146401 (2010).
[37] M. Eckstein and P. Werner, Phys. Rev. B **82**, 115115 (2010).
[38] N. Grewe and H. Keiter, Phys. Rev. B **24**, 4420 (1981).
[39] P. Coleman, Phys. Rev. B **29**, 3035 (1984).
[40] D. Golež, M. Eckstein, and P. Werner, Phys. Rev. B **92**, 195123 (2015).
[41] T. Pruschke and N. Grewe, Z. Phys. B **74**, 439 (1989).
[42] K. Haule, S. Kirchner, J. Kroha, and P. Wölfle, Phys. Rev. B **64**, 155111 (2001).
[43] R. Sensarma, D. Pekker, E. Altman, E. Demler, N. Strohmaier, D. Greif, R. Jördens, L. Tarruell, H. Moritz, and T. Esslinger, Phys. Rev. B **82**, 224302 (2010).
[44] Z. Lenarčič and P. Prelovšek, Phys. Rev. Lett. **111**, 016401 (2013).

[45] P. Werner, K. Held, and M. Eckstein, Phys. Rev. B **90**, 235102 (2014).
[46] For all two-time quantities $O(t,t')$ we define the partial Fourier transform as $O(t,\omega)=\int_t^{t+t_{\rm cut}} dt' e^{i\omega(t'-t)}O(t',t)$, with $t_{\rm cut}=7$, which allows us to compute the spectrum with a time-independent resolution up to relatively long times. We checked that this choice of cutoff does not qualitatively affect the dynamics of the spectral properties under consideration.
[47] An further increased nonlocal interaction strength $V$ would eventually lead to the condensation of the bosonic modes at $(\pi,\pi)$ and the formation of charge order.
[48] N. Tsuji, T. Oka, and H. Aoki, Phys. Rev. Lett. **103**, 047403 (2009).
[49] N. Tsuji, Ph.D. dissertation, University of Tokyo, 2010.
[50] J. E. Hirsch, Phys. Rev. Lett. **87**, 206402 (2001).
[51] P. Werner and M. Eckstein, Struct. Dyn. **3**, 023603 (2016).
[52] A. Kogar, S. Vig, Y. Gan, and P. Abbamonte, J. Phys. B **47**, 124034 (2014).
[53] H. Ibach and D. L. Mills, *Electron Energy Loss Spectroscopy and Surface Vibrations* (Academic, New York, 2013).
[54] Z. Lenarčič, D. Golež, J. Bonča, and P. Prelovšek, Phys. Rev. B **89**, 125123 (2014).